Rotary Encoder-based Health Indicators for Early Detection of Gear Pitting in Commercial Gearboxes

Toby Verwimp[1,2], Rui Zhu[1,2], Hao Wen[1,2], Achilleas Achilleos[1,2], and Konstantinos Gryllias[1,2]

[1] *LMSD Division Mecha(tro)nic System Dynamics, Department of Mechanical Engineering, KU Leuven, Celestijnenlaan 300, Box 2420, 3001 Leuven, Belgium*

toby.verwimp@kuleuven.be
rui.zhu@kuleuven.be
hao.wen@kuleuven.be
achilleas.achilleos@kuleuven.be
konstantinos.gryllias@kuleuven.be

[2] *Flanders Make @ KU Leuven, Leuven, Belgium*

ABSTRACT

This paper investigates the diagnostic capabilities of rotary encoders for condition monitoring of commercial gearboxes, focusing on early detection of gear pitting. Within a multi-sensor framework, rotary encoder data were collected alongside accelerometer signals, both mounted on a multi-stage commercial gearbox subjected to gear pitting. Encoder-based health indicators were developed from the synchronously averaged (SA) transmission error (TE) and its square envelope (SE). By automatically capturing images of a gear during an accelerated life test, these indicators were evaluated for their ability to detect the onset of gear pitting and compared against conventional vibration-based indicators. Results show that encoder-based indicators can provide earlier and more consistent detection of gear pitting. These findings highlight the potential of rotary encoders as a complementary or standalone sensing solution in advanced diagnostic frameworks for commercial gearboxes.

1. INTRODUCTION

Gearboxes are critical components in a wide range of industrial applications, including manufacturing, transportation, energy, and heavy machinery. Their reliable operation is essential for minimizing downtime and maintaining overall system efficiency. Among the various failure modes that affect gearboxes, gear pitting—a surface fatigue phenomenon characterized by the formation of small pits on gear tooth surfaces—is one of the most common (Sheng, 2014). Left undetected, pitting can progress rapidly, eventually leading to gear tooth fracture, excessive vibration, and ultimately catastrophic system failure.

Condition monitoring, and in particular fault detection, techniques have been widely studied to detect such faults early and enable predictive maintenance. Among these, vibration analysis using accelerometers has become the de facto standard in industrial gearbox health monitoring. Accelerometer-based approaches typically involve time-domain, frequency-domain, and time-frequency domain signal processing techniques (Lee, Shim, & Cho, 2006; Elasha et al., 2014; Bechhoefer & Butterworth, 2019).

Alongside vibration measurements, signals from other sensors used in machine control and performance monitoring - such as rotary encoders - have been increasingly explored for fault detection (Zhao & Lin, 2018). Besides their function in position and speed control of industrial machinery, these sensors offer several advantages over vibration sensors (e.g, accelerometers). First, being directly connected to a rotating component, they provide a shorter and simpler transfer path compared to vibration signals transmitted through bearings and casings. Second, they capture torsional behavior and may be more sensitive to stiffness losses caused by defects. Third, since many rotating machines (e.g., wind turbines) operate under variable speeds, direct or indirect speed measurements help avoid the smearing of characteristic frequencies tied to rotation. Finally, the angle-time relationship is naturally sampled in the angle domain, where gear and bearing faults manifest at specific angles, facilitating defect localization.

Over the past years, numerous studies have explored different quantities (e.g., transmission error, instantaneous angular speed, instantaneous angular acceleration) derived from rotary encoder signals for fault detection and diagnosis for

bearings (Renaudin, Bonnardot, Musy, Doray, & Rémond, 2010; Bourdon, Chesné, André, & Rémond, 2019), gears (Zhao, Jia, Lin, Lei, & Lee, 2018; Liang, Liu, Kong, Li, & Xu, 2019), or even motors and pumps (Yang, Pu, Wang, Zhou, & Yan, 2001; Verwimp, Mousmoulis, Gryllias, & Hajnayeb, 2023). For gears in particular, transmission error (TE) has been originally studied in gear transmission modelling to improve transmission performance (Harris, 1958; Palermo, Britte, Janssens, Mundo, & Desmet, 2018). Nowadays, it is also widely studied for gear fault detection and wear assessment (Koch, Sendlbeck, Otto, Stahl, & Kirchner, 2025; Mahfoudh & Rémond, 2009; Randall, Chin, Smith, & Borghesani, 2019; Chin, Smith, Borghesani, Randall, & Peng, 2021; Chin, Borghesani, Mao, Smith, & Randall, 2022; Chin, Borghesani, Smith, Randall, & Peng, 2023; Mao, Tong, Chin, Borghesani, & Peng, 2023; Liu et al., 2023).

Despite the growing interest in encoder-based diagnostics, most existing studies cover artificial faults in single-stage custom-made gearboxes (Koch et al., 2025). Literature lacks systematic investigations on the performance of encoder-based health indicators applied to long-term tests, which allow going beyond a simple comparison between healthy and faulty gears by including the full fault progression (Koch et al., 2025). Furthermore, encoder-based diagnostics are still underexplored, especially in commercial multi-stage helical gearboxes. Last but not least, systematic comparisons between encoder-based health indicators and conventional vibration-based metrics remain limited, even not published (Koch et al., 2025), especially under controlled fault progression scenarios.

This paper addresses these gaps by presenting a novel framework for early detection of gear pitting using rotary encoder signals. Within a multi-sensor experimental setup, both high-resolution rotary encoders and accelerometers are installed on a commercial multi-stage gearbox subjected to an accelerated life test. Encoder-based health indicators are derived from synchronously averaged (SA) TE signals, isolating the contribution of the targeted gear, and their square envelope (SE). The progression of gear pitting is automatically documented using high-resolution imaging, allowing for the comparison of the health indicators against the actual fault progression. Performance of the proposed indicators is benchmarked against traditional vibration-based metrics to assess their relative effectiveness and robustness in detecting early-stage pitting.

More specifically, the paper continues with an explanation of the TE measurement principle and the proposed methodology in Section 2. Section 3 describes the experimental setup and the dataset used for validation. The application of the methodology and analysis of the results are presented in Section 4. Finally, conclusions are drawn in Section 5.

2. METHODOLOGY

2.1. Transmission Error Measurement

Gear TE is defined as the difference between the actual gearwheel's angular position with respect to the pinion and the position it would have if the gear transmission were perfect (i.e., perfectly rigid bodies and conjugated teeth profiles) (Rémond, 1998). The angle θ_{in} of the input shaft (with pinion) and the angle θ_{out} of the output shaft (with gear) can be measured using high-resolution rotary encoders mounted on the respective shafts and the pulse timing method: every time the encoder (with R angle increments per revolution) generates a pulse, the time is recorded using a high-frequency clock (Li et al., 2005; André, Girardin, Bourdon, Antoni, & Rémond, 2014). This results in the time-angle relations $t(\theta_{in})$ and $t(\theta_{out})$. Using time as the common variable for synchronous measurements, the angle-time relations $\theta_{in}(t)$ and $\theta_{out}(t)$ are obtained by interpolation to one of the time series $t(\theta_{in})$ or $t(\theta_{out})$ (Rémond & Mahfoudh, 2005). The TE [rad] is calculated as (here with the input shaft as reference):

$$TE(\theta_{in}) = \theta_{in}(t) - i\theta_{out}(t) \quad (1)$$

$$= \theta_{in}(t) - i\theta_{out}(t(\theta_{in})) \quad (2)$$

where i is the gear ratio of the gear pair. Figure 1 shows as a function of time t the voltages V_{in} and V_{out} generated by the encoders on the input and output shaft respectively, the high-frequency clock signal V_{clock}, and the time-angle relations.

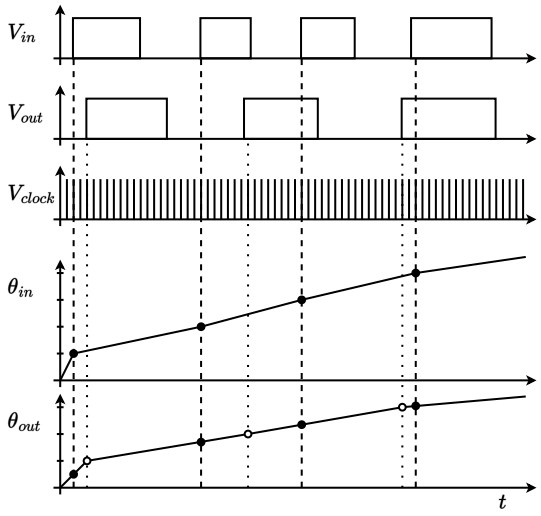

Figure 1. Schematic of the transmission error measurement principle: the voltages V_{in} and V_{out} generated by the encoders on the input and output shaft respectively, the high-frequency clock signal V_{clock}, and the time-angle relations $t(\theta_{in})$ and $t(\theta_{out})$. The solid dots represent the sampled time stamps for each encoder independently, while the hollow dots represent the interpolated time stamps to obtain $\theta_{out}(t(\theta_{in}))$.

2.2. Proposed Indicators

Above TE measurement principle is typically applied to a single gear pair, having an encoder on each shaft. In this work, the TE measurement principle is applied to a commercial multi-stage gearbox, in which not all shafts are accessible to mount encoders, but only the input and output shaft. In this case, the measured TE is a combination of the TE of all gear pairs in the gearbox. An attempt to isolate the contribution of a specific gear pair is made by synchronously averaging (SA) the TE signal with respect to the shaft on which the gear of interest is located. Similar to vibration signals, the TE signals are expected to contain amplitude and frequency-modulated components (Feki, Cavoret, Ville, & Velex, 2013).

A first set of indicators is derived from the order spectrum of this SA TE signal: the sideband index (SI), and the sideband energy ratio (SER), both using one gear mesh order (GMO) and one pair of sidebands (Antolick, Branning, Wade, & Dempsey, 2010; Hanna, Hatch, Kalb, Weiss, & Luo, 2012):

$$S_k = \mathcal{F}\{TE_k(\theta_{in})\} \tag{3}$$

$$SI_k = \frac{S_{k,GMO-SO} + S_{k,GMO+SO}}{2} \tag{4}$$

$$SER_k = \frac{S_{k,GMO-SO} + S_{k,GMO+SO}}{S_{k,GMO}} \tag{5}$$

with $TE_k(\theta_{in})$ the SA TE signal with respect to shaft k, $S_{k,GMO}$ the amplitude of the GMO, $S_{k,GMO-SO}$ and $S_{k,GMO+SO}$ the amplitudes of the lower and upper sideband respectively in the order spectrum S_k of the SA TE signal, and SO the shaft order corresponding to the shaft on which the gear of interest is located.

Then, to demodulate the SA TE signal, the square envelope is computed using the Hilbert transform (HT) in Eq. (7), resulting in a second set of indicators. The Gini index (GI) of the square envelope is applied to the SA TE signal (of which the mean is subtracted) in order to emphasize impulsive bursts related to local defects such as pitting, while being also robust against random outliers (Fan, Guo, & Yin, 2025; Miao, Wang, Zhang, & Li, 2022; Wang, 2018):

$$z_k(\theta_{in}) = TE_k(\theta_{in}) - jH[TE_k(\theta_{in})], \quad j = \sqrt{-1} \tag{6}$$

$$SE_k(\theta_{in}) = |z_k(\theta_{in})|^2 = TE_k^2(\theta_{in}) + H(TE_k(\theta_{in}))^2 \tag{7}$$

$$GI_k = 1 - \frac{2}{N-1} \sum_{n=1}^{N} \frac{SE_k(n)}{\|SE_k\|_1} \left(\frac{N-n+0.5}{N} \right) \tag{8}$$

$H[\cdot]$ represents the HT. The sample index n ranges from 1 to N, the number of samples in the SA TE signal, and $\|SE_k\|_1$ is the $L1$ norm of the square envelope signal. The GI ranges from 0 to 1, where 0 indicates a perfectly uniform distribution (no impulsiveness) and 1 indicates maximum inequality (highly impulsive).

Finally, the square envelope spectrum (SES) of the SA TE signal is computed (i.e., the order spectrum of the square envelope), and different (sum of) amplitudes are extracted as indicators (Zhu, Van Maele, Poletto, De Baets, & Gryllias, 2024):

$$SES_k = \mathcal{F}\{SE_k(\theta_{in})\} \tag{9}$$

$$ASO\ (SES_k) = SES_k(SO) \tag{10}$$

$$SSO\ (SES_k) = \sum_{p=1}^{5} SES_k(p\ SO) \tag{11}$$

$$AGMO\ (SES_k) = SES_k(GMO) \tag{12}$$

$$SGMO\ (SES_k) = \sum_{q=1}^{3} SES_k(q\ GMO) \tag{13}$$

The above steps are also shown in Fig. 2.

2.3. Evaluating Indicators

Besides visual inspection of the indicators over a full test, their performance needs to be evaluated quantitatively. In this work, their fault detection performance is evaluated as follows.

Similar to the approach in (Zhu et al., 2024), a set of acquisitions during the healthy operation of the gearbox is selected to compute a threshold for each indicator, based on the median absolute deviation (MAD). Then, it is checked when an indicator exceeds this threshold. To avoid false alarms, a moving window is used and an alarm is only raised when the following two conditions are met: (1) the indicator continuously exceeds the threshold for 50 % (or more) of the acquisitions in the moving window, and (2) the average indicator value in the moving window is equal or greater than the threshold. The delay between the fault onset (i.e., the first observation of a pit on the gear tooth surface) and the first alarm is used to evaluate and compare the detection performance of the different indicators.

As some indicators might seem to perform well, their success might be due to the selected healthy period. Therefore, a sensitivity analysis is performed using a Monte Carlo approach: the healthy period is randomly selected multiple times (typ-

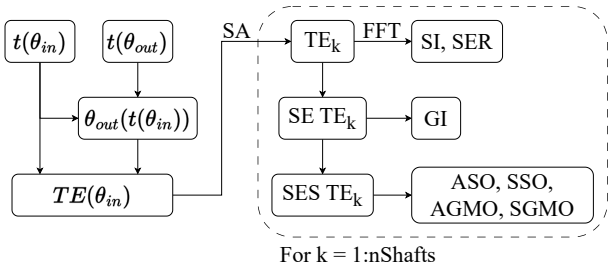

Figure 2. Schematic of the proposed methodology.

ically a thousand iterations), while considering a minimum number of acquisitions and ensuring the selected acquisitions are not too close to the fault onset. For each randomly selected healthy period, the above detection procedure is applied and the delay between fault onset and first alarm is stored. The distribution of these delays is used to evaluate the robustness of the detection performance of the different indicators, by comparing their box plots.

3. DESCRIPTION OF THE TEST RIG AND DATASET

3.1. Test Rig Description

An accelerated life test was conducted on an electric power circulated back-to-back gearbox setup at KU Leuven. As shown from left to right in Fig. 3a, the test rig consists of an induction motor A, a test gearbox, a torque transducer, a drive gearbox, and an induction motor B, connected to each other through flexible couplings. Motor A rotates the setup while motor B is used to apply load. Two variable frequency drives (VFD) are used to closed-loop control the speed of motor A using a rotary encoder mounted on its shaft, and the torque applied by motor B using the torque transducer (Kistler 4503B). This back-to-back configuration allows for using a relatively small motor B to apply a large load on the output shaft of the test gearbox. The test and drive gearboxes have two helical gear stages and have a gear ratio of 49.12 and 48.76, respectively. The number of gear teeth in the test gearbox is 10, 103, 13, and 62 for the input pinion, input gear, output pinion, and output gear, respectively, as shown in Fig. 3b. The bearings in the different components are omitted to keep the drawing clear.

3.2. Sensors and Data Acquisition

The test gearbox is equipped with PT100 oil temperature sensors (SICK TSP) and two triaxial piezo-electric accelerometers (PCB Piezotronics J356A45). An optical rotary incremental encoder (Hengxiang PN58) with 4096 pulses per revolution (ppr) is installed on the input shaft and another one (Hengxiang K66) with 10000 ppr is installed on the output shaft. The position of the accelerometers and encoders is shown in Fig. 3b. Measurements from the accelerometers and the torque transducer were acquired at a sampling frequency of 51.2 kHz using a Simcenter SCADAS Mobile data acquisition system. Simultaneously with the former, the encoder signals were sampled in the angle domain (with the ET method) using a counter frequency of 820 MHz of the same system. Every 10 minutes, signals from the above sensors (accelerometers, encoders, and temperature sensors) were recorded for 12 s.

Additionally, images of the second stage pinion were captured every hour using a vision system mounted above the test gearbox, in order to monitor the surface condition of the gear. In this way it is possible to have a ground-truth for the surface condition of the gear, which is used to evaluate the performance of the developed health indicators. The vision system consists of a camera (Teledyne DALSA Falcon 4 CLHS and accessories), a lens (ZEISS Interlock 2/50), and a light source (CCS LNLP). Furthermore, to have visual access to the second stage pinion, the gearbox lid was replaced with a mechanism that allows for opening and closing the gearbox and some air nozzles were installed to clean the gear teeth before capturing images (but after meshing) and to protect the lens from upcoming oil droplets through an air curtain.

3.3. Accelerated Life Test

An accelerated life test was conducted on the test gearbox, where the input shaft was rotated at a constant speed of about 2600 rpm while the output shaft was loaded with a gradually increasing torque throughout the full test. In this paper we only focus on the last load stage, which was the application of a torque of about 300 Nm for about 7.5 days. During this last period the gearbox experienced gear pitting on the second stage pinion. At the end of the last load stage, the intermediate shaft fractured, causing the test to stop.

Fig. 4 shows the operating conditions as a function of the number of revolutions (cycles) of the input shaft during this last load stage of the accelerated life test. Furthermore, the test was stopped a couple of times to do some checks (black dotted lines), and sometimes no images were captured (gray shaded areas). For the analysis in Section 4, the six acquisitions after a restart of the test are not considered, as the resulting indicators might be affected by the increasing temperature during this hour. Additionally, Fig. 4 shows two important moments during the test (indicated by pink dotted lines): at about 12.5 million cycles in this load stage the first symptoms of contact fatigue were observed on the second stage pinion with a small pit on one tooth flank. At about 23 million cycles, small pits were observed on three tooth flanks, indicating the progression of the pitting fault. For the latter moment, this is observed once reactivating the vision system after it was off since about 20 million cycles. Therefore the progression of the pitting to three tooth flanks happened between 20 and 23 million cycles. Finally, in Fig. 4 and all subsequent figures showing the evolution of a quantity/indicator over the test, the final 1.1 million cycles are not displayed, as the indicator values increase sharply just before the intermediate shaft fracture and would compress the earlier trends associated with the smaller pitting damages.

4. APPLICATION OF THE METHODOLOGY AND ANALYSIS OF THE RESULTS

4.1. Application to a Healthy and Faulty Case

Before applying the proposed methodology to the full test described above, it is first applied to a healthy and a faulty case. The healthy case corresponds to an acquisition at the begin-

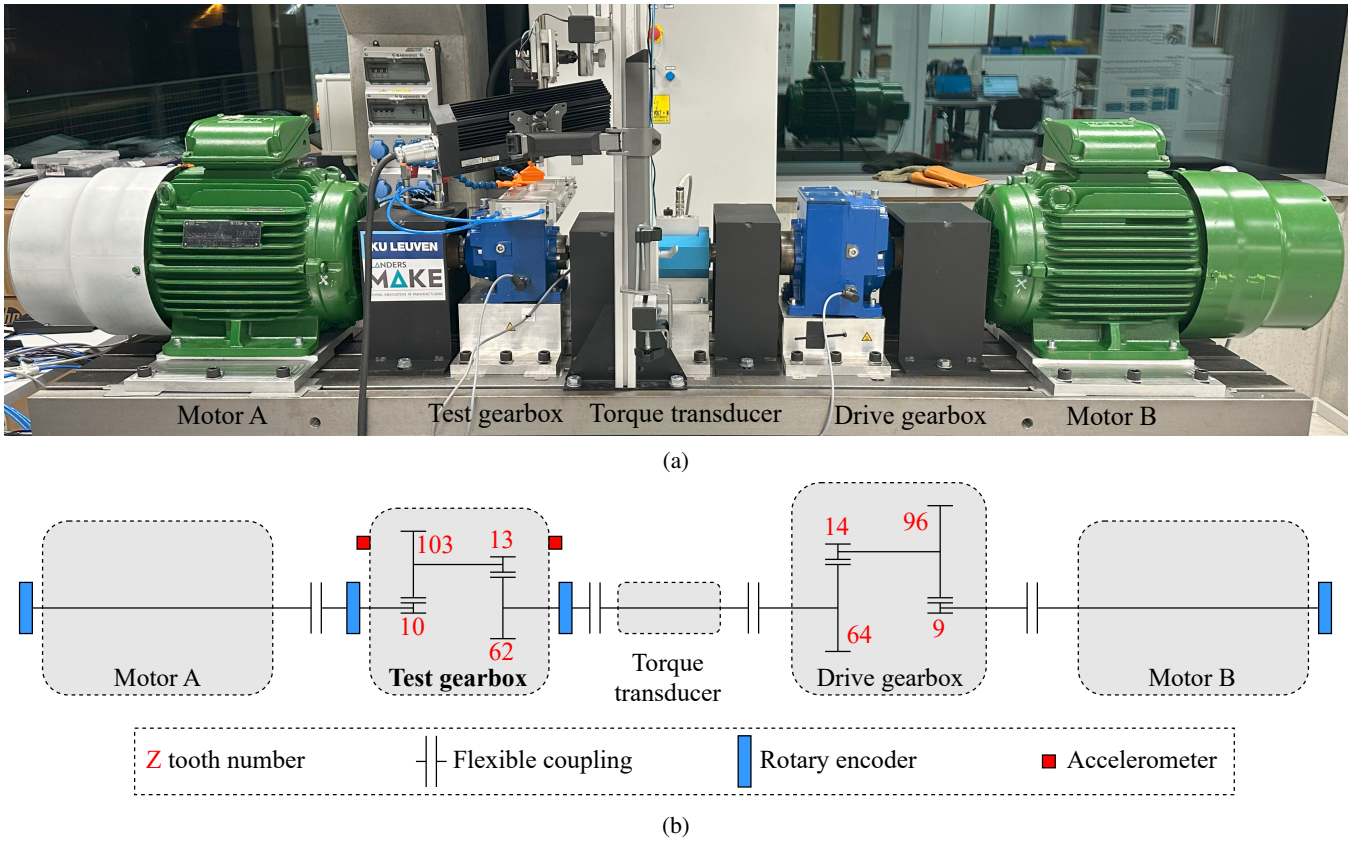

Figure 3. (a) Picture and (b) kinematic diagram (including sensor positions) of the back-to-back gearbox test rig at KU Leuven.

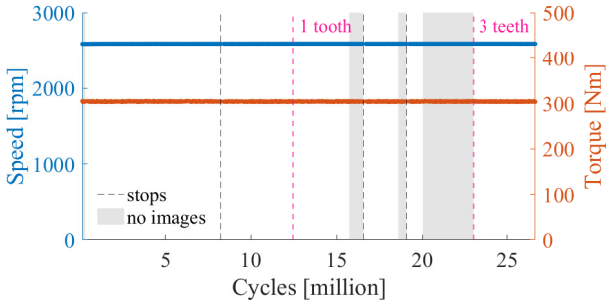

Figure 4. Operating conditions during the last load stage of the accelerated life test: speed and torque measured at the input and output shaft, respectively.

ning of the last load stage (at about 10 million cycles), while the faulty case corresponds to an acquisition after the pitting initiation (at about 15 million cycles).

The angle, TE, and SA TE signals for both cases are shown in Fig. 5, in the left and right column respectively. During the acquisition, the input shaft completes about 517 revolutions, while the output shaft completes about 10.5 revolutions, which corresponds to the gear ratio of 49.12. Figures 5e and 5f are zoomed in to two rotations of the low-speed (output) shaft. The SA TE signals for each shaft are dominated by the shaft order, caused by eccentricity or misalignment, even present in healthy conditions. Furthermore, the TE and SA TE signals have almost the same shape and amplitude for both cases, making fault detection based on these signals very challenging.

Therefore, the SE and SES of the SA TE signals for the intermediate shaft (i.e., shaft 2, with the targeted gear) are computed, and are shown in Fig. 6. The SE signals are plotted for one revolution of the intermediate shaft (i.e., 10.3 revolutions of the input shaft), and the corresponding order spectrum (SES) is shown up to order 5, but goes up to order 2048 (i.e., half the angular sampling frequency of 4096 ppr). The SE signals have a similar shape, but for the faulty case the amplitude is higher than for the healthy case. This is due to the presence of the pit, which causes an increase in the number and amplitude of the SO sidebands around the GMO in the order spectrum of the SA TE signal. This is reflected as an increase in the shaft order (i.e., 0.097 with respect to the input shaft) in the SE, which is also observed in the SES in Fig. 6d with respect to Fig. 6c. The GMO (i.e., 1.26 with respect to the input shaft) is not affected by the presence of the pit.

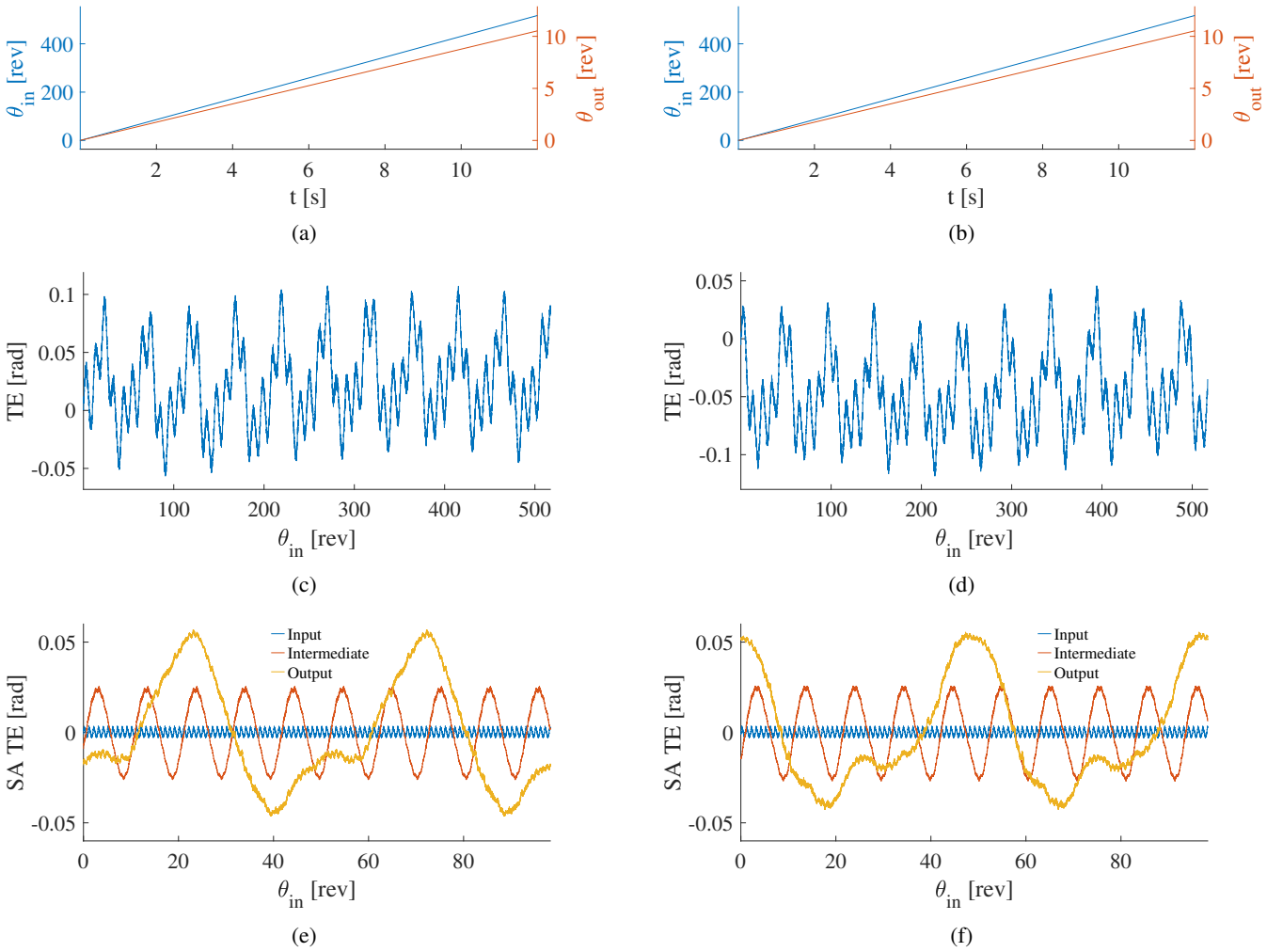

Figure 5. Application of the proposed methodology to a healthy case (left column) and a faulty case (right column): (a,b) Angle-TE signals, (c,d) TE signals, and (e,f) SA TE signals of the SA TE signals.

4.2. Application to the Full Test

After showing the results for a healthy and a faulty case, the proposed methodology is applied to all acquisitions of the last load stage of the accelerated life test, described in Section 3.3.

The indicators derived from the SA TE signal (SI and SER), the SE-based indicator (GI), and the SES-based indicators (ASO, SSO, AGMO, and SGMO) are shown in Fig. 7 as a function of the number of cycles of the input shaft. Most indicators show a trend related to the progression of the pitting fault, with a change in behavior around the moments where the first pit and later three pits were observed on the second stage pinion (indicated by pink dotted lines). The SE-based GI (Fig. 7c), and SES-based ASO (Fig. 7d) and SSO (Fig. 7e) show an increase after the first pit was observed and another increase is observed when three pitted teeth occur in the interval between 20 and 23 million cycles, which indicates that these indicators are sensitive to the initiation and progression of the pitting fault. The SI (Fig. 7a) and SER (Fig. 7b) indicators also show an increasing trend, but mostly after three pitted teeth were observed. Therefore, these indicators seem less sensitive to the initiation of small pits, but they can still capture the fault once more pits are present. The SES-based AGMO (Fig. 7f) and SGMO (Fig. 7g) show a stable or slightly decreasing trend. Only when the three pitted teeth occur, their trend is going upwards.

To quantitatively evaluate the fault detection performance of the different indicators, the procedure described in Section 2.3 is applied. An example of the thresholding and detection procedure is shown in Fig. 8 for the SE-based GI indicator of Fig. 7c. The selected healthy period consists of the first 100 acquisitions (i.e. up to about 2.7 million cycles). The threshold (horizontal dashed line) is computed based on the MAD of the GI values in this healthy period. Then, a moving window of 10 acquisitions is used to check when the two con-

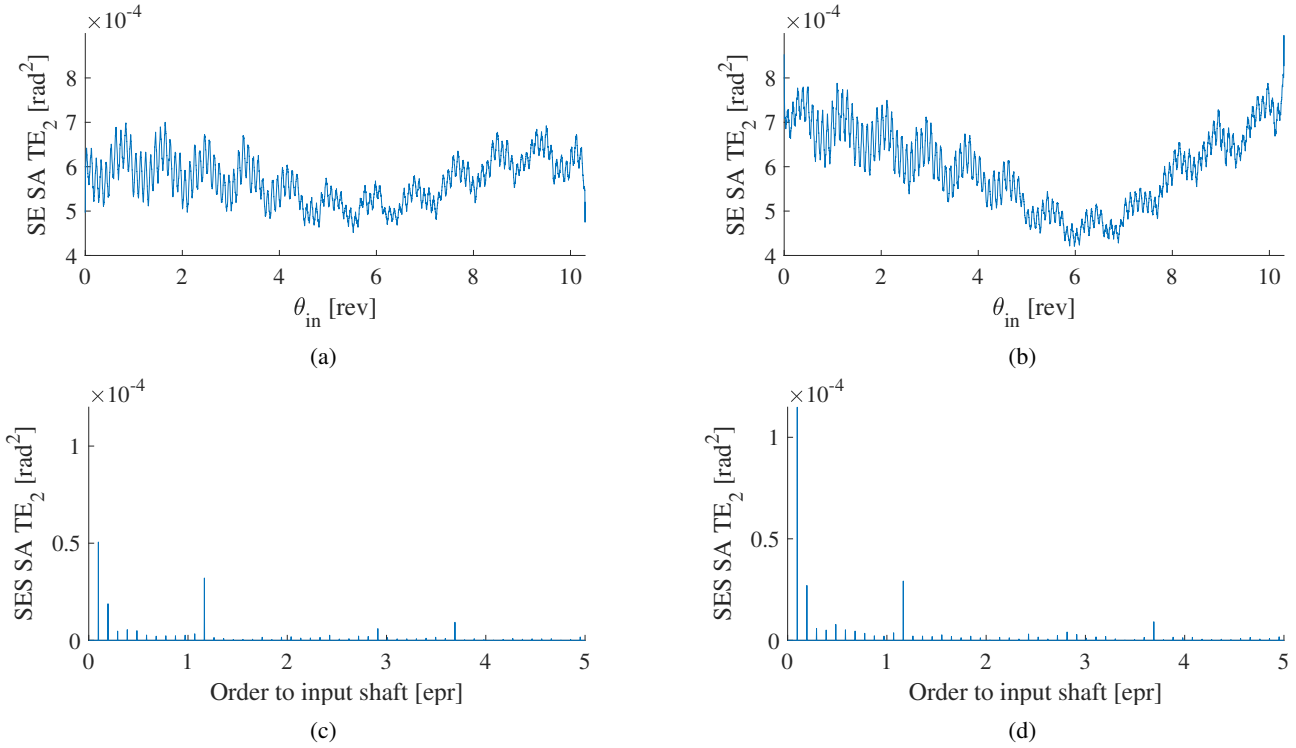

Figure 6. Application of the proposed methodology to a healthy case (left column) and a faulty case (right column) (cont.): (a,b) square envelope (SE) of the SA TE signals, and (c,d) square envelope spectrum (SES) of the SA TE signals.

ditions for raising an alarm are met (vertical red dashed line). In this case, the alarm is raised at about 13.8 million cycles, resulting in a delay of about 1.4 million cycles after the fault onset (first observation of a pit on the gear tooth surface).

The sensitivity analysis using a Monte Carlo approach is performed by randomly selecting a healthy period 10000 times. The minimum number of acquisitions in the healthy period is set to 20, and the last acquisition to be considered is acquisition number 400 (i.e., about 10.7 million cycles). The results of this sensitivity analysis are summarized using box plots in Fig. 9. The median is indicated by the red line and the blue box represents the interquartile range (IQR). The whiskers extend to the minimum and maximum, so they represent the whole range of alarm delays. The results show that the SE-based GI and SES-based ASO and SSO indicators have the best fault detection performance, with a median delay of about 1.4, 0.7, and 0.9 million cycles, respectively. Furthermore, the IQR for SES ASO shows that this delay is the same for 50 % of the random selections of the healthy period. Together with a limited range, this indicator has a quite robust fault detection performance. The SI and SER indicators have a quite large median delay of about 10.7 and 8.5 million cycles, respectively. The SES-based AGMO and SGMO indicators have a median delay of about 12.5 and 12.3 million cycles, respectively, which is even larger.

4.3. Comparison with Vibration-based Indicators

To benchmark the performance of the proposed TE-based indicators, the same detection procedure is applied to vibration-based indicators derived from the axial channel of the triaxial accelerometer mounted on the gearbox housing close to the second stage (see Fig. 3b).

The considered vibration-based indicators are: (a) traditional indicators like the root mean square (RMS) value, the kurtosis, the sideband index (SI), and the sideband energy ratio (SER), (b) indicators proposed by NASA like the fourth order figure of merit (FM4), the sixth order normalized statistical moment (M6A), the fourth order normalized statistical moment (NA4), and the eighth order normalized statistical moment (M8A) (Sharma & Parey, 2016), and (c) the SES-based indicators like the amplitude at the shaft frequency (ASF), the sum of the first five harmonics of the shaft frequency (SSF), the amplitude at the gear mesh frequency (AGMF), and the sum of the first three harmonics of the gear mesh frequency (SGMF) (Zhu et al., 2024). The latter indicators are similar to the SES-based indicators derived from the TE signal, but they are computed based on the frequency spectrum of the raw vibration signal instead of the order spectrum of the SA TE signal.

The evolution of these groups of vibration-based indicators are shown in Figs. 11, 12, and 13 in the appendix, while their

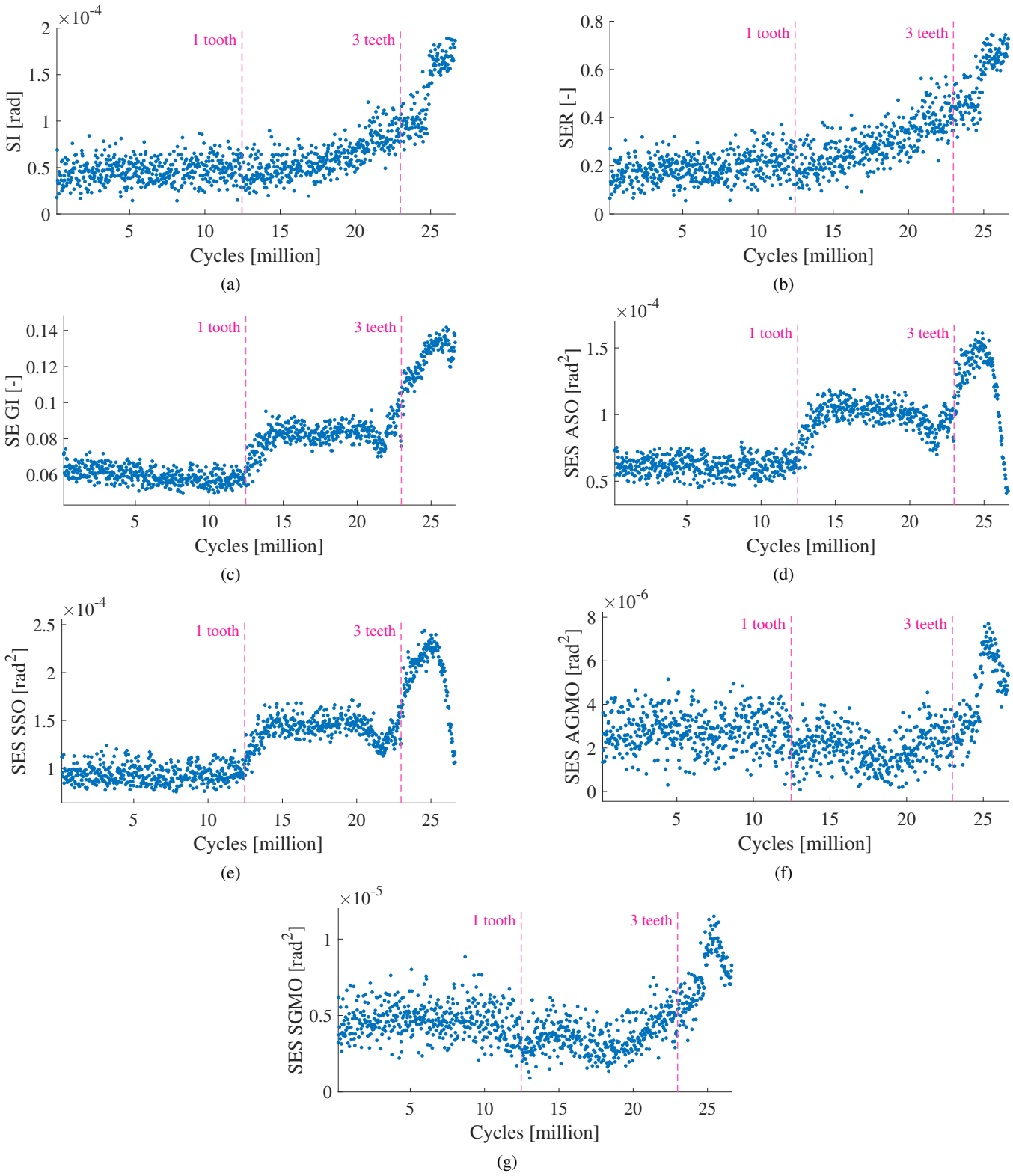

Figure 7. Evolution of the TE-based indicators: (a) SI, (b) SER, (c) GI, (d) ASO, (e) SSO, (f) AGMO, and (g) SGMO.

fault detection performance is summarized using box plots in Fig. 10. For some vibration-based indicators, the detection procedure did not result in an alarm for some selections of the healthy period. In that case, the alarm is set to the maximum

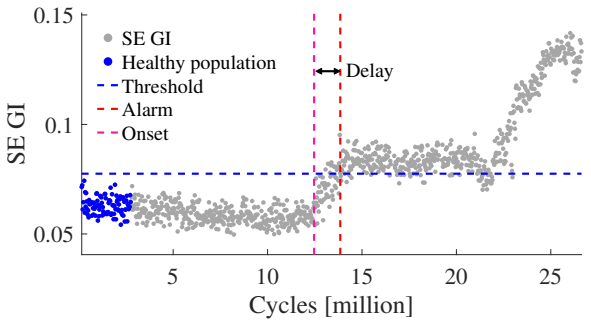

Figure 8. Example of the thresholding and detection procedure for the SE GI indicator of Fig. 7c.

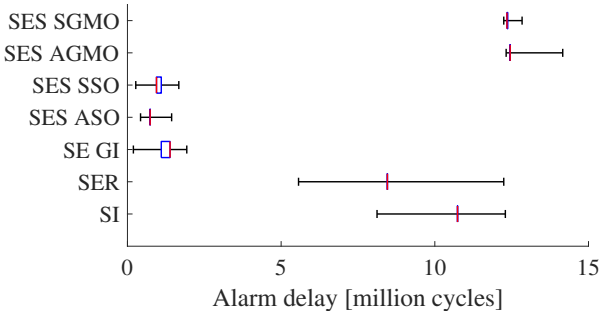

Figure 9. Box plots of the delay between fault onset and alarm for the different TE-based indicators, using a Monte Carlo approach with 10000 random selections of the healthy period.

number of cycles in the last load stage (i.e., about 26.6 million cycles or about 14.2 million cycles after the fault onset).

Figure 10 shows that the kurtosis, SI, SER, SES AGMF, and SES SGMF indicators have the worst fault detection performance: they detect the fault very late (or not at all). The SES ASF and SSF indicators have a median delay of about 6.2 and 5.3 million cycles, respectively, which is still quite large, compared to their TE-based counterparts. The RMS, FM4, M6A, NA4, and M8A indicators have the best fault detection performance among the vibration-based indicators, with a median delay between 1.6 and 2.5 million cycles. However, for the RMS, and NA4, the IQR is very large, indicating that their fault detection performance is not robust. The FM4, M6A, and M8A indicators have a more robust fault detection performance, but they still lag behind the best-performing TE-based indicators (SE GI, SES ASO, and SES SSO).

Even more, the range of most vibration-based indicators is very large compared to the TE-based indicators, and most of them also have false alarms (i.e., negative delay), while the TE-based indicators do not have any false alarms. This is due to the observation that the encoder-based indicators have a more stable behavior than the vibration-based indicators during healthy operation, as can be seen by comparing the healthy periods in Fig. 7 with the ones in Figs. 11, 12, and 13 in the appendix. For a stable indicator during healthy operation, the selection of the healthy period has less influence on the computed threshold, resulting in a more robust fault detection performance.

4.4. Discussion

The above comparison highlights the advantages of TE-based indicators over vibration-based indicators in terms of early and robust fault detection. To further contextualize these findings, this section discusses the underlying reasons for these advantages, compares the proposed TE-based indicators with other encoder-based approaches, and reflects on practical implementation aspects.

The main reason for the more stable behavior of the TE-based indicators compared to the vibration-based indicators is that the vibration signals are acquired via an accelerometer mounted on the gearbox housing, which suffers from long and complex transmission paths between the source (i.e., the gear mesh) and the sensor. These transmission paths are affected by various factors, such as mounting conditions, structural resonances, and environmental noise, which can introduce variability and instability in the measured vibration signals. On the other hand, the TE signals are derived directly from the incremental encoders mounted on the gearbox shafts, providing a more direct measurement of the gear meshing behavior with less influence from external factors. This direct measurement leads to more consistent and reliable indicators for condition monitoring.

Although this work focuses on early and robust gear pitting detection, it has to be noted that some SES-based indicators are decreasing from 25 to 26.6 million cycles. This is probably related to the intermediate shaft being partially cracked, which influences the investigated dynamics. The combination of this phenomenon with gear pitting needs to be further investigated.

Besides the vibration-based approaches, there are also other encoder-based approaches for condition monitoring of gearboxes in the literature. For instance, some studies focus on analyzing the instantaneous angular speed or instantaneous angular acceleration derived from a single encoder signal. Although these approaches have been shown to be effective for fault detection in rotating machinery, especially gearboxes, they are less sensitive for small cracks or initial pitting faults compared to TE-based approaches. The measurements from a single encoder are affected by manufacturing or installation errors, making fault detection more challenging. In contrast, the computation of the TE signal from dual-shaft encoder measurements allows for canceling common excitation sources, leading to a more accurate representation of the gear meshing behavior and improved fault detection sensitivity (Liang et al., 2019).

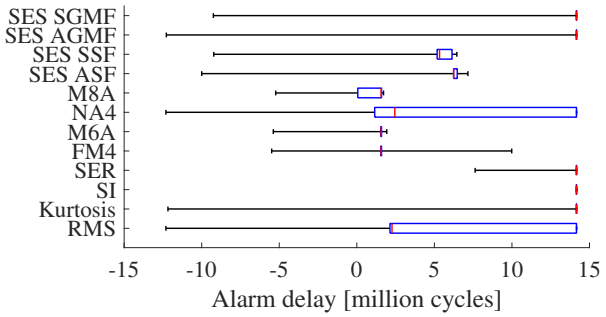

Figure 10. Box plots of the delay between fault onset and alarm for the different vibration-based indicators, using a Monte Carlo approach with 10000 random selections of the healthy period.

Although the encoder-based indicators show a better fault detection performance compared to the vibration-based indicators in this accelerated life test, it is important to reflect on the practical aspects of using encoders for condition monitoring of gearboxes. First of all, the high-resolution incremental encoders used in this study were selected to fit the small available space on the input and output shaft of the gearbox, but in existing industrial applications, encoders are typically mounted on the motor shafts (for speed control purposes) rather than on the gearbox shafts, and these existing applications typically do not allow retrofitting encoders on the gearbox shafts, as this typically requires disassembling the drivetrain. Nevertheless, retrofittable angle sensors (e.g., zebra tapes with optical sensors or magnetic encoders) could be an alternative to install encoders on the gearbox shafts without disassembling the drivetrain. In contrast to typical rotary encoders, accelerometers are more commonly used for condition monitoring of gearboxes in industrial applications, as they can be easily mounted on the gearbox housing without disassembling the drivetrain. Regarding cost, high-resolution incremental encoders can be more expensive than accelerometers, especially when considering the total cost of installation, but nowadays, the cost difference is not as significant as it used to be, due to advancements in encoder technology.

From the above, one can conclude that further investigation is needed to evaluate the performance of the proposed methodology when using encoder signals from motor-mounted encoders. It is expected to have a somewhat lower performance, as the TE signal (or any other quantity derived from the encoder measurements) will be dampened by the drivetrain components (especially flexible couplings) between the motor and the gearbox. The performance of retrofittable angle sensors (e.g., zebra tapes with optical sensors) should also be evaluated in future work, with the advantage of being able to install them on the gearbox shafts without disassembling the drivetrain, but with the disadvantage of a lower resolution compared to typical rotary encoders.

5. CONCLUSION

In this paper, a novel methodology for condition monitoring of multi-stage gearboxes using incremental encoders is proposed. The methodology consists of computing the TE signal from the encoder signals, applying a synchronous average to isolate the contribution of a specific shaft and the gears mounted on it, and extracting several indicators from the SA TE signal, its SE, and its SES. The proposed methodology is applied to an accelerated life test of a two-stage gearbox, where gear pitting occurred on the second stage pinion. The results show that some of the proposed TE-based indicators are not only sensitive to the initiation, but also to the progression of the pitting fault. A quantitative evaluation of their fault detection performance using a Monte Carlo approach shows that the SE-based GI and SES-based ASO and SSO indicators have the best performance. Furthermore, the SES ASO indicator has a robust fault detection performance, with the smallest IQR and range. The performance of the proposed TE-based indicators is benchmarked against several traditional, NASA, and SES-based vibration indicators derived from an accelerometer mounted on the gearbox. The results show that the best-performing vibration-based indicators (i.e., FM4, M6A, and M8A) have a larger median delay and range compared to the best-performing TE-based indicators. Furthermore, most vibration-based indicators have false alarms, while the TE-based indicators do not have any false alarms. This is due to the more stable behavior of the TE-based indicators during healthy operation, which results in a more robust fault detection performance. Therefore, it can be concluded that incremental encoders are a valuable additional sensor for condition monitoring of gearboxes, next to accelerometers. Future work will focus on: (a) applying and evaluating the proposed methodology to other datasets, including other test rigs, (b) evaluating the fault size tracking performance of the indicators, (c) using the encoder signals acquired from encoders mounted on the motors, instead of on the gearbox shafts, which is more common in industrial applications, and (d) investigating the use of retrofittable angle sensors (e.g., zebra tapes with optical sensors) for condition monitoring of gearboxes.

ACKNOWLEDGMENT

This work was supported by Flanders Make, the strategic research center for the manufacturing industry, in the context of the QED project. Additionally, the authors would like to gratefully acknowledge the support of the China Scholarship Council and the support of the Fonds Wetenschappelijk Onderzoek Vlaanderen (FWO) under the research grants no. 1SE0125N and G0A3123N, and under the travel grant no. K1AG025N.

REFERENCES

André, H., Girardin, F., Bourdon, A., Antoni, J., & Rémond, D. (2014). Precision of the IAS monitoring system based on the elapsed time method in the spectral domain. *Mechanical Systems and Signal Processing*, *44*(1), 14-30. doi: 10.1016/j.ymssp.2013.06.020

Antolick, L. J., Branning, J. S., Wade, D. R., & Dempsey, P. J. (2010). Evaluation of gear condition indicator performance on rotorcraft fleet. In *AHS 66th Annual Forum and Technology Display: Rising to New Heights in Vertical Lift Technology.* Phoenix, AZ, United States.

Bechhoefer, E., & Butterworth, B. (2019). A comprehensive analysis of the performance of gear fault detection algorithms. In *Proceedings of the Annual Conference of the PHM Society 2019* (Vol. 11). Prognostics and Health Management Society. doi: 10.36001/phmconf.2019.v11i1.823

Bourdon, A., Chesné, S., André, H., & Rémond, D. (2019). Reconstruction of angular speed variations in the angular domain to diagnose and quantify taper roller bearing outer race fault. *Mechanical Systems and Signal Processing*, *120*, 1-15. doi: 10.1016/j.ymssp.2018.09.040

Chin, Z. Y., Borghesani, P., Mao, Y., Smith, W. A., & Randall, R. B. (2022). Use of transmission error for a quantitative estimation of root-crack severity in gears. *Mechanical Systems and Signal Processing*, *171*, 108957. doi: 10.1016/j.ymssp.2022.108957

Chin, Z. Y., Borghesani, P., Smith, W. A., Randall, R. B., & Peng, Z. (2023). Monitoring gear wear with transmission error. *Wear*, *523*, 204803. doi: 10.1016/j.wear.2023.204803

Chin, Z. Y., Smith, W. A., Borghesani, P., Randall, R. B., & Peng, Z. (2021). Absolute transmission error: A simple new tool for assessing gear wear. *Mechanical Systems and Signal Processing*, *146*, 107070. doi: 10.1016/j.ymssp.2020.107070

Elasha, F., Ruiz-Cárcel, C., Mba, D., Kiat, G., Nze, I., & Yebra, G. (2014). Pitting detection in worm gearboxes with vibration analysis. *Engineering Failure Analysis*, *42*, 366-376. doi: 10.1016/j.engfailanal.2014.04.028

Fan, J., Guo, Y., & Yin, X. (2025). Instantaneous angular speed based fault detection for planet and cycloidal gears in rotary vector reducers. *IEEE Transactions on Instrumentation and Measurement*, *74*, 1-10. doi: 10.1109/TIM.2025.3542103

Feki, N., Cavoret, J., Ville, F., & Velex, P. (2013). Detection of gear tooth pitting based on transmission error measurements. In M. Haddar, L. Romdhane, J. Louati, & A. B. Amara (Eds.), *Proceedings of the Fifth International Conference Design and Modeling of Mechanical Systems, CMSM* (p. 181-188). Berlin, Heidelberg: Springer Berlin Heidelberg. doi: 10.1007/978-3-642-37143-1

Hanna, J., Hatch, C., Kalb, M., Weiss, A., & Luo, H. (2012). Detection of wind turbine gear tooth defects using sideband energy ratio™. *China Wind Power*, *32*.

Harris, S. L. (1958). Dynamic loads on the teeth of spur gears. *Proceedings of the Institution of Mechanical Engineers*, *172*(1), 87-112. doi: 10.1243/PIME-PROC-1958-172-017-02

Koch, Y., Sendlbeck, S., Otto, M., Stahl, K., & Kirchner, E. (2025). A review on the use of angle measurements in gear condition monitoring and fault detection. *Mechanical Systems and Signal Processing*, *225*, 112254. doi: 10.1016/j.ymssp.2024.112254

Lee, S. K., Shim, J. S., & Cho, B. O. (2006). Damage detection of a gear with initial pitting using the zoomed phase map of continuous wavelet transform. *Key Engineering Materials*, *306-308*, 223-228. doi: 10.4028/www.scientific.net/KEM.306-308.223

Li, Y., Gu, F., Harris, G., Ball, A., Bennett, N., & Travis, K. (2005). The measurement of instantaneous angular speed. *Mechanical Systems and Signal Processing*, *19*(4), 786-805. doi: 10.1016/j.ymssp.2004.04.003

Liang, L., Liu, F., Kong, X., Li, M., & Xu, G. (2019). Application of instantaneous rotational speed to detect gearbox faults based on double encoders. *Chinese Journal of Mechanical Engineering*, *32*(9). doi: 10.1186/s10033-019-0324-z

Liu, H., Lin, J., Jiao, J., Zhang, B., Liu, Z., & Lu, X. (2023). A differential diagnosis approach of localized planet gear fault using overall transmission error. *Measurement*, *222*, 113647. doi: 10.1016/j.measurement.2023.113647

Mahfoudh, J., & Rémond, D. (2009). Experimental study of the transmission error for the detection of gear faults. In *Proceedings of the ASME Turbo Expo 2003, collocated with the 2003 International Joint Power Generation Conference* (Vol. 1, p. 345-349). Atlanta, Georgia, USA: American Society of Mechanical Engineers (ASME). doi: 10.1115/GT2003-38289

Mao, Y., Tong, J., Chin, Y., Borghesani, P., & Peng, Z. (2023). Transmission-error- and vibration-based condition monitoring of gear wear with contaminated lubricant. *Wear*, *523*, 204760. doi: 10.1016/j.wear.2023.204760

Miao, Y., Wang, J., Zhang, B., & Li, H. (2022). Practical framework of gini index in the application of machinery fault feature extraction. *Mechanical Systems and Signal Processing*, *165*, 108333. doi: 10.1016/j.ymssp.2021.108333

Palermo, A., Britte, L., Janssens, K., Mundo, D., & Desmet, W. (2018). The measurement of gear transmission error as an NVH indicator: Theoretical discussion and industrial application via low-cost digital encoders to an all-electric vehicle gearbox. *Mechanical Systems and Signal Processing*, *110*, 368-389. doi:

10.1016/j.ymssp.2018.03.005

Randall, R. B., Chin, Z. Y., Smith, W. A., & Borghesani, P. (2019). Measurement and use of transmission error for diagnostics of gears. In *Surveillance, Vishno and AVE conferences.* INSA-Lyon, Université de Lyon, Lyon, France.

Renaudin, L., Bonnardot, F., Musy, O., Doray, J. B., & Rémond, D. (2010). Natural roller bearing fault detection by angular measurement of true instantaneous angular speed. *Mechanical Systems and Signal Processing*, *24*(7), 1998-2011. doi: 10.1016/j.ymssp.2010.05.005

Rémond, D. (1998). Practical performances of high-speed measurement of gear transmission error or torsional vibrations with optical encoders. *Measurement Science and Technology*, *9*(3), 347-353. doi: 10.1088/0957-0233/9/3/006

Rémond, D., & Mahfoudh, J. (2005). From transmission error measurements to angular sampling in rotating machines with discrete geometry. *Shock and Vibration*, *12*(2), 149-161. doi: 10.1155/2005/205291

Sharma, V., & Parey, A. (2016). A review of gear fault diagnosis using various condition indicators. *Procedia Engineering*, *144*, 253-263. doi: 10.1016/j.proeng.2016.05.131

Sheng, S. (2014). *Gearbox typical failure modes, detection, and mitigation methods (Presentation): NREL (National Renewable Energy Laboratory)* (Other No. NREL/PR-5000-60982). National Renewable Energy Lab (NREL), Golden, CO (United States).

Verwimp, T., Mousmoulis, G., Gryllias, K., & Hajnayeb, A. (2023). Cavitation detection based on instantaneous angular speed. In *19th International Conference on Condition Monitoring and Asset Management, CM 2023.* The British Institute of Non-Destructive Testing. doi: 10.1784/CM2023.2E1

Wang, D. (2018). Some further thoughts about spectral kurtosis, spectral L2/L1 norm, spectral smoothness index and spectral Gini index for characterizing repetitive transients. *Mechanical Systems and Signal Processing*, *108*, 360-368. doi: 10.1016/j.ymssp.2018.02.034

Yang, J., Pu, L., Wang, Z., Zhou, Y., & Yan, X. (2001). Fault detection in a diesel engine by analysing the instantaneous angular speed. *Mechanical Systems and Signal Processing*, *15*(3), 549-564. doi: 10.1006/mssp.2000.1344

Zhao, M., Jia, X., Lin, J., Lei, Y., & Lee, J. (2018). Instantaneous speed jitter detection via encoder signal and its application for the diagnosis of planetary gearbox. *Mechanical Systems and Signal Processing*, *98*, 16-31. doi: 10.1016/j.ymssp.2017.04.033

Zhao, M., & Lin, J. (2018). Health assessment of rotating machinery using a rotary encoder. *IEEE Transactions on Industrial Electronics*, *65*(3), 2548-2556. doi: 10.1109/TIE.2017.2739689

Zhu, R., Van Maele, D., Poletto, J. C., De Baets, P., & Gryllias, K. (2024). Development and evaluation of vibration indicators for gear pitting detection. In *International Conference on Noise and Vibration Engineering (ISMA 2024) and International Conference on Uncertainty in Structural Dynamics (USD 2024)* (pp. 508–521). Katholieke Universiteit Leuven, Department of Mechanical Engineering.

BIOGRAPHIES

Toby Verwimp received his MSc in mechanical engineering from KU Leuven, Leuven, Belgium in 2021. He joined the LMSD (Mecha(tro)nic System Dynamics) Division in the Department of Mechanical Engineering at KU Leuven as a PhD researcher in 2021. His research interests include condition monitoring of rotating machinery using, among others, rotary encoders and cameras.

Rui Zhu received his MSc in Mechanical Engineering from Southeast University, China, in 2019. Since 2020, he has been a PhD researcher in the LMSD (Mecha(tro)nic System Dynamics) Division of the Department of Mechanical Engineering at KU Leuven. His research interests focus on condition monitoring of rotating machinery with advanced signal processing methodologies.

Hao Wen received his Bachelor of Science degree from the China University of Geosciences, China and his Master of Science degree in Mechanical Engineering from the University of Manchester, UK. He joined the LMSD (Mecha(tro)nic System Dynamics) Division in the Department of Mechanical Engineering at KU Leuven as a PhD researcher in 2022. His research interests lie in the areas of fault detection utilizing unsupervised learning and generative modeling.

Achilleas Achilleos received his Diploma in Mechanical Engineering from the National Technical University of Athens, Athens, Greece, in 2021. He joined the LMSD (Mecha(tro)nic System Dynamics) Division in the Department of Mechanical Engineering at KU Leuven as a PhD researcher in 2024. His research interests include dynamic gear modeling and condition monitoring in rotating machinery.

Konstantinos Gryllias received his Diploma and Ph.D. degrees in Mechanical Engineering from the National Technical University of Athens, Athens, Greece, in 2004 and 2010, respectively. He is currently Professor of Vibro-acoustics of machines and transportation systems at the Department of Mechanical Engineering,KU Leuven, Leuven, Belgium. He also serves as the Manager of the University Core Lab Flanders Make@KU Leuven Motion Products,

Belgium. His research interests include condition monitoring, signal processing, prognostics, and health management of mechanical and mechatronic systems.

APPENDIX

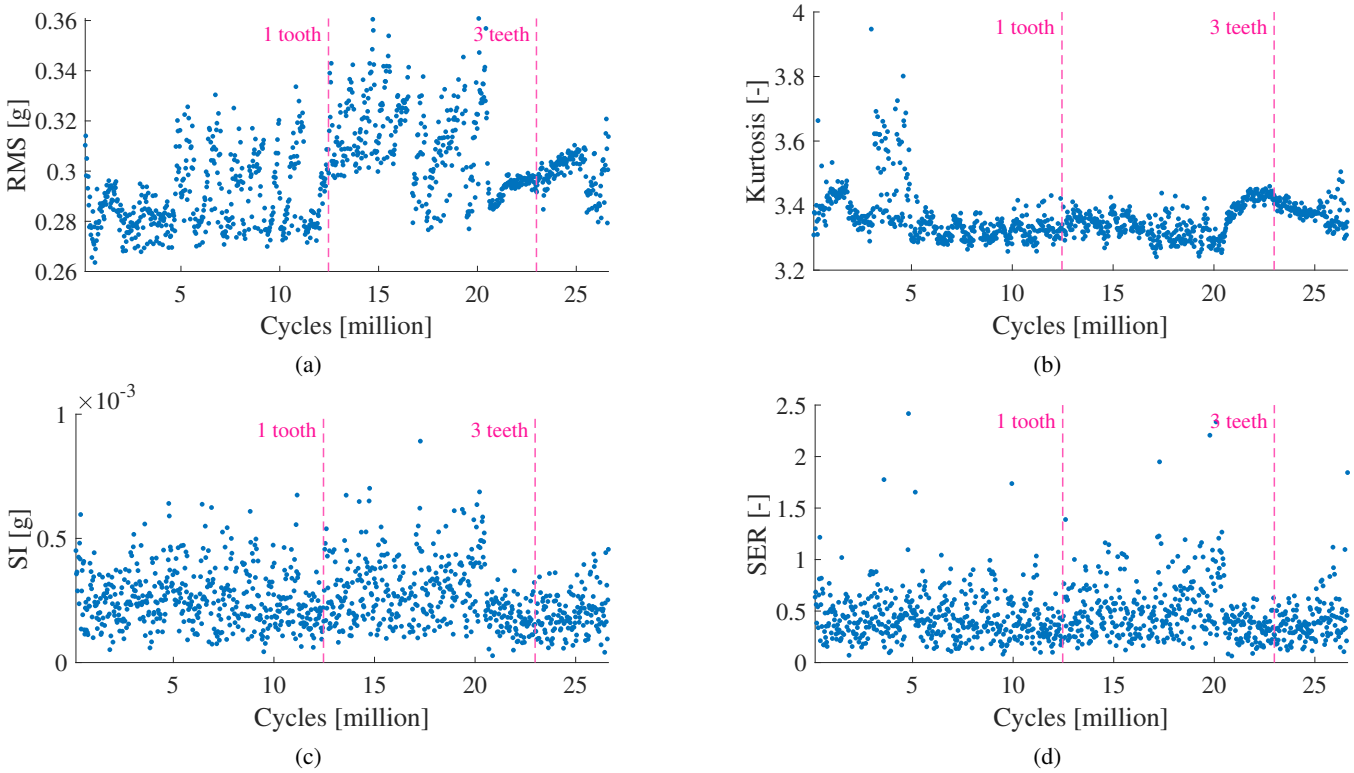

Figure 11. Evolution of the traditional vibration-based indicators: (a) RMS, (b) kurtosis, (c) SI, and (d) SER.

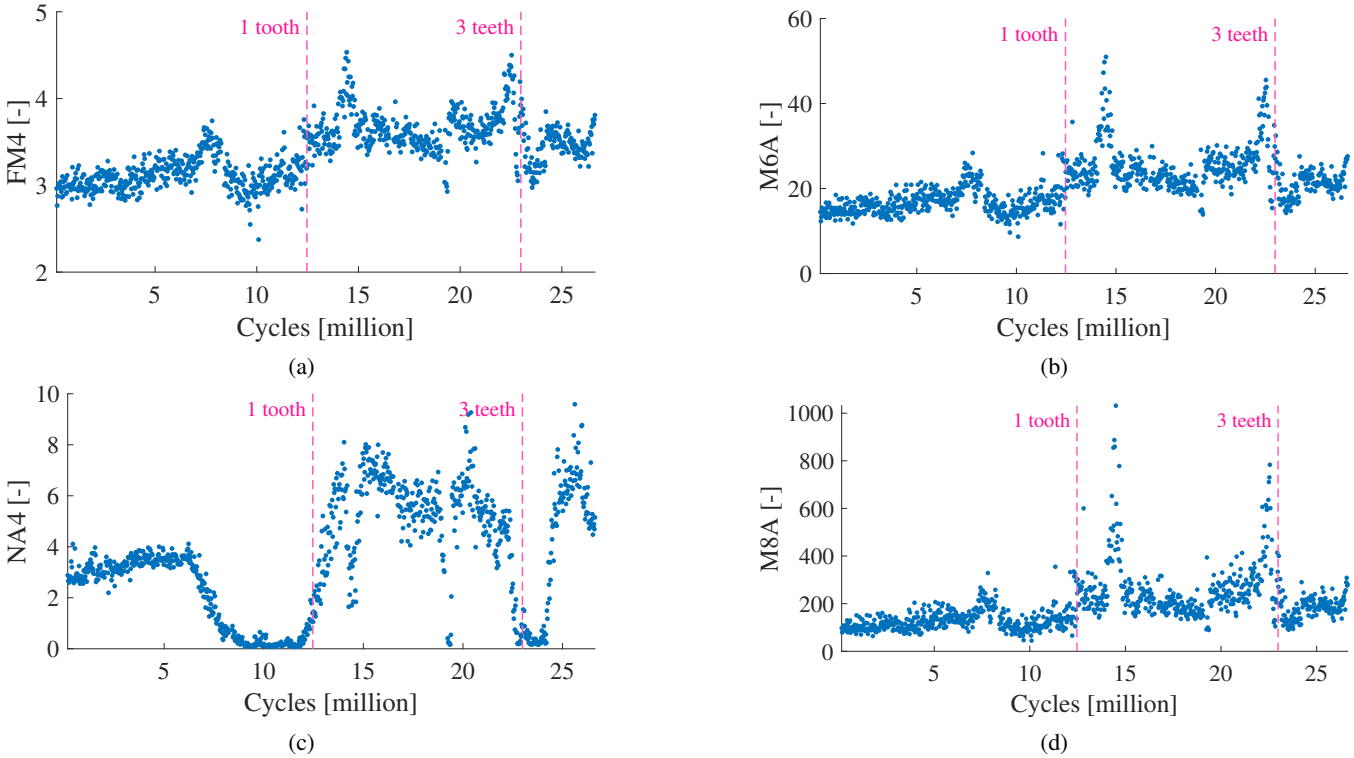

Figure 12. Evolution of the NASA vibration-based indicators: (a) FM4, (b) M6A, (c) NA4, and (d) M8A.

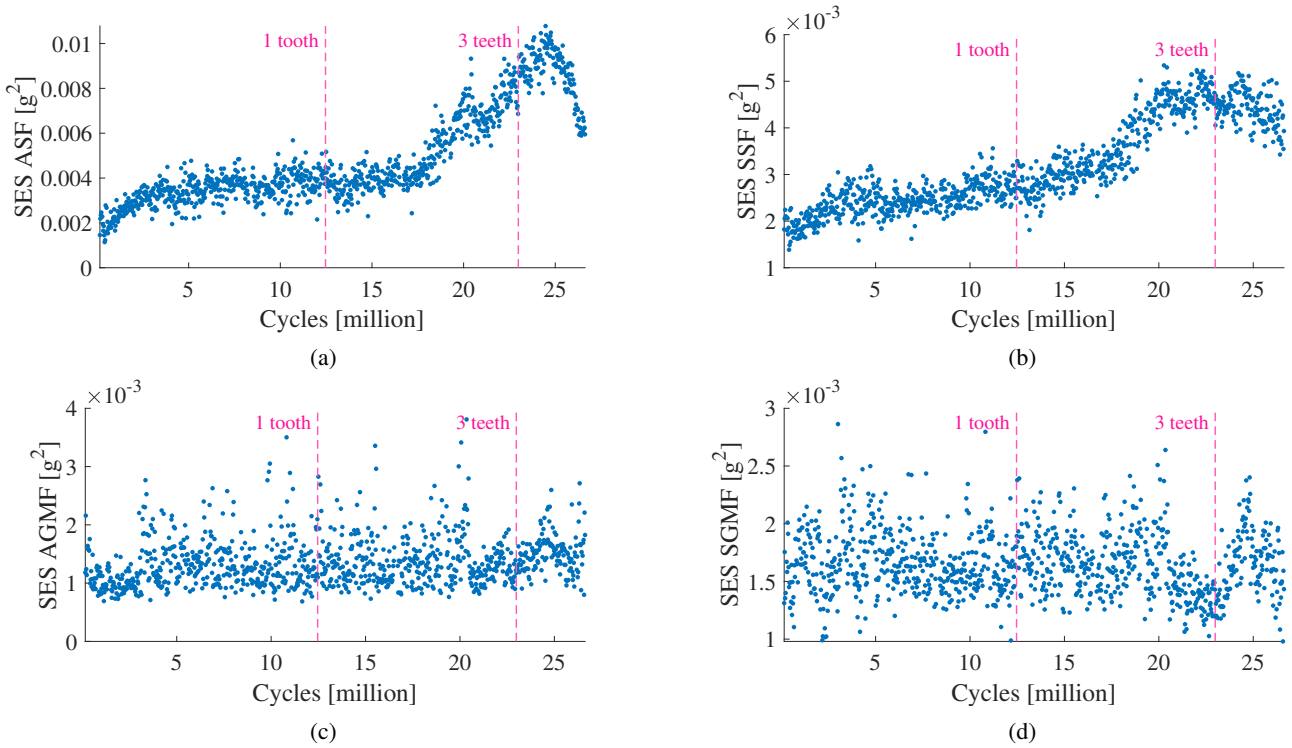

Figure 13. Evolution of the SES-based vibration indicators: (a) ASF, (b) SSF, (c) AGMF, and (d) SGMF.